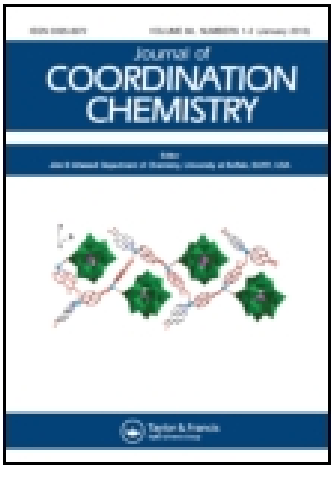

Journal of Coordination Chemistry
Publication details, including instructions for authors and subscription information:
http://www.tandfonline.com/loi/gcoo20

Stereospecific π-π stacking interactions between pseudo-enantiomeric sulfur-bridged dinuclear Co(III)-Pd(II) and Co(III)-Pt(II) complexes with optically active propanediamines

Toshihiro Nagasaki[a], Yusuke Miyoshi[a], Masayuki Koikawa[a] & Yasunori Yamada[a]

[a] Department of Chemistry and Applied Chemistry, Graduate School of Science and Engineering, Saga University, Saga, Japan

Accepted author version posted online: 29 Apr 2014.Published online: 22 May 2014.

Journal of Coordination Chemistry, 2014
Vol. 67, No. 9, 1639–1651, http://dx.doi.org/10.1080/00958972.2014.919387

Stereospecific π–π stacking interactions between pseudo-enantiomeric sulfur-bridged dinuclear Co(III)–Pd(II) and Co(III)–Pt(II) complexes with optically active propanediamines

TOSHIHIRO NAGASAKI, YUSUKE MIYOSHI, MASAYUKI KOIKAWA and YASUNORI YAMADA*

Department of Chemistry and Applied Chemistry, Graduate School of Science and Engineering, Saga University, Saga, Japan

(*Received 11 September 2013; accepted 21 March 2014*)

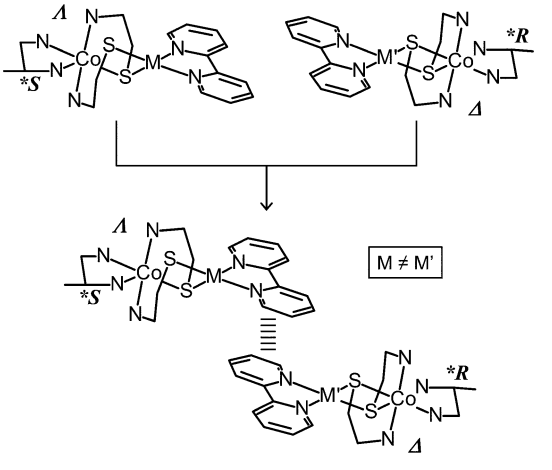

Assemblies between pseudo-enantiomers with different d^8 metal centers, Δ-[M(bpy){Co(aet)$_2$(*R*-pn)}]$^{3+}$ (M = Pd or Pt, bpy = 2,2′-bipyridine, aet = 2-aminoethanethiolate, pn = 1,2-propanediamine), and Λ-[M′(bpy){Co(aet)$_2$(*S*-pn)}]$^{3+}$ (M′ ≠ M, M′ = Pd or Pt), have been examined from stereo- and spectrochemical aspects. A mixture of equimolar amounts of the optically active sulfur-bridged dinuclear complex, Δ-[M(bpy){Co(aet)$_2$(*R*-pn)}](NO$_3$)$_3$·7H$_2$O, and its pseudo-enantiomer, Λ-[M′(bpy){Co(aet)$_2$(*S*-pn)}](NO$_3$)$_3$·7H$_2$O, in H$_2$O crystallizes as [M(bpy){Co(aet)$_2$(*R*-pn)}][M′(bpy){Co(aet)$_2$(*S*-pn)}](NO$_3$)$_6$·4H$_2$O, in which two complex cations with imperfect enantiomorphisms form a 1 : 1 π–π stacked unit.

Keywords: Stereospecific interactions; Pseudo-enantiomers; Co(III)–Pd(II) and Co(III)–Pt(II) complexes; 1,2-Propanediamine; Crystal structures; Spectrochemistry

*Corresponding author. Email: yyamada@cc.saga-u.ac.jp

1. Introduction

It has been demonstrated that an octahedrally coordinated metal chelated by multiple β-aminoalkylthiolate ligands acts as a S-donating bidentate metalloligand toward $[MX_2(bpy)]$ (M = Pd(II) or Pt(II), $X = Cl^-$ or NO_3^-, and bpy = 2,2′-bipyridine), in which the two X^- ligands are labile toward substitution by other ligands, resulting in the formation of a dinuclear complex composed of a $[M(\mu\text{-}S)_2(bpy)]$ framework and an octahedral metal unit [1–7]. In the reaction of *fac(S)*-$[Co(aet)_3]$ (aet = 2-aminoethanethiolate) with $[PtCl_2(bpy)]$, for instance, a dinuclear dication, $[Pt(bpy)\{Co(aet)_3\}]^{2+}$, is formed [1]. A similar reaction of $[Ni\{Co(aet)_2(en)\}_2]^{4+}$ (en = ethylenediamine), in which the two terminal *cis(S)*-$[Co(aet)_2(en)]^+$ units can be regarded as bidentate S-donors, with $[PtCl_2(bpy)]$ gives $[Pt(bpy)\{Co(aet)_2(en)\}]^{3+}$ [1]. Two absolute configurations, Δ and Λ, are possible for such octahedral S-donating metal units and, hence, these dinuclear complexes are obtained as racemic crystals. In contrast to the above racemic $[Ni\{Co(aet)_2(en)\}_2]^{4+}$, an optically active trinuclear analog, ΔΔ-$[Ni\{Co(aet)_2(R\text{-pn})\}_2]^{4+}$ (pn = 1,2-propanediamine), reacts with $[MX_2(bpy)]$ to form Δ-$[M(bpy)\{Co(aet)_2(R\text{-pn})\}]^{3+}$ stereoselectively [2, 3]. A similar optically active S-bridged dinuclear complex, $[M(bpy)\{Co(D\text{-pen})_2\}]^+$ (pen = penicillaminate), is preferentially derived from the bidentate metalloligand, *trans(N,O,S)*-$[Co(D\text{-pen})_2]$ [3]. While these optically active complexes exist as monomers in the crystalline state, the racemic complexes afford dimeric or long linear-chain structures due to *π–π* stacking of the bpy frameworks in the dinuclear units [1–7]. This implies enantioselective interactions between the *π* frameworks, which are rather distant from the chiral center of the octahedral metal unit in these dinuclear complexes. In fact, an equimolar mixture of Δ-$[Pt(bpy)\{Co(aet)_2(R\text{-pn})\}]X_3$ ($X = NO_3^-$ or ClO_4^-) and Λ-$[Pt(bpy)\{Co(aet)_2(S\text{-pn})\}]X_3$ crystallizes from an aqueous solution as racemic $[Pt(bpy)\{Co(aet)_2(R\text{-pn})\}]_{0.5}[Pt(bpy)\{Co(aet)_2(S\text{-pn})\}]_{0.5}X_3$ with a dimeric *π–π* stacking structure between the two enantiomeric complex cations [5]. In the same way, racemic $[Pt(bpy)\{Co(D\text{-pen})_2\}]_{0.5}[Pt(bpy)\{Co(L\text{-pen})_2\}]_{0.5}Cl$, with a linear-chain *π–π* stacking structure in which the two enantiomeric complex cations are arranged alternatingly, preferentially crystallizes from an aqueous solution containing equimolar amounts of $[Pt(bpy)\{Co(D\text{-pen})_2\}]Cl$ and $[Pt(bpy)\{Co(L\text{-pen})_2\}]Cl$ [4]. Providing such stereospecific interactions is applicable between optically active complexes with imperfect enantiomorphisms, it leads the way to methodological development in the construction of assemblies with heterometallic building blocks. Furthermore, the resulting assemblies could promise combined and concerted functions from the building-blocks. In the present investigation, we have examined assemblies between pseudo-enantiomers with different d^8 metal centers, Δ-$[M(bpy)\{Co(aet)_2(R\text{-pn})\}]^{3+}$ (M = Pd or Pt) and Λ-$[M'(bpy)\{Co(aet)_2(S\text{-pn})\}]^{3+}$ (M′ ≠ M, M′ = Pd or Pt), from stereo- and spectrochemical aspects.

2. Experimental

2.1. *Materials*

2-Aminoethanethiol hydrochloride, 2,2′-bipyridine, 1,2-propanediamine, L-(+)-tartaric acid, $AgNO_3$, $Ca(OH)_2$, $CoCl_2{\cdot}6H_2O$, $PdCl_2$, and K_2PtCl_4 were commercially available and were used as received. ΔΔ-$[Ni\{Co(aet)_2(R\text{-pn})\}_2]Cl_4{\cdot}6H_2O$, ΛΛ-$[Ni\{Co(aet)_2(S\text{-pn})\}_2]Cl_4{\cdot}6H_2O$, $[PdCl_2(bpy)]$, and $[PtCl_2(bpy)]$ were prepared using the modified literature

methods [5, 8–11]. Δ-[Pt(bpy){Co(aet)$_2$(*R*-pn)}](NO$_3$)$_3$·7H$_2$O (***R*Pt**·7H$_2$O) and Λ-[Pt(bpy){Co(aet)$_2$(*S*-pn)}](NO$_3$)$_3$·7H$_2$O (***S*Pt**·7H$_2$O) were synthesized by previously reported procedures [5].

2.2. *Preparation of Δ-[Pd(bpy){Co(aet)$_2$(R-pn)}](NO$_3$)$_3$ (RPd)*

This complex was prepared by a method similar to that used for ***R*Pt**·7H$_2$O [5] using [PdCl$_2$(bpy)] instead of [PtCl$_2$(bpy)]. [PdCl$_2$(bpy)] (0.17 g, 0.5 mM) was added to a reddish brown solution of ΔΔ-[Ni{Co(aet)$_2$(*R*-pn)}$_2$]Cl$_4$·6H$_2$O (0.22 g, 0.25 mM) in 50 cm^3 of H$_2$O. The reaction was stirred at 55 °C for 1 h, whereupon it became dark red. The solution was cooled to room temperature and AgNO$_3$ (0.34 g, 2 mM) in 5 cm^3 of H$_2$O was added. After removing precipitated AgCl by filtration, the filtrate was evaporated to one-tenth of its original volume under reduced pressure. After the addition of ca. 20 cm^3 acetone, the solution was allowed to stand at 25 °C for several days. The resulting dark red microcrystalline powder (0.31 g, 72% yield based on Co) was collected by filtration. Anal. Calcd for C$_{17}$H$_{44}$N$_9$O$_{16}$S$_2$CoPd (***R*Pd**·7H$_2$O): C, 23.74; H, 5.16; N, 14.66%. Found: C, 23.76; H, 5.15; N, 14.60%. ^{1}H NMR (300 MHz, D$_2$O), $\delta = 1.40$ (s, 3H, pn), 2.15 (t, 2H, $J = 13.9$ Hz, aet), 2.43 (t, 1H, $J = 13.6$ Hz, pn), 2.63 (d, 2H, $J = 13.9$ Hz, aet), 3.00 (d, 2H, $J = 13.7$ Hz, pn), 3.52 (d, 2H, $J = 13.6$ Hz, aet), 3.66 (t, 2H, $J = 13.2$ Hz, aet), 7.83 (t, 2H, $J = 6.0$ Hz, bpy), 8.33 (t, 2H, $J = 7.9$ Hz, bpy), 8.43 (d, 2H, $J = 7.9$ Hz, bpy), 8.91 (d, 2H, $J = 5.3$ Hz, bpy). UV–Vis spectrum in H$_2$O [ν_{max}, 10^3 cm^{-1} (log ε/M^{-1} dm^3 cm^{-1})]: 20.00 (2.41), 26.1 (3.2)$^{sh\ (shoulder)}$, 29.5 (3.9)^{sh}, 31.1 (4.3)^{sh}, 32.47 (4.40), 35.7 (4.3)^{sh}, 43.9 (4.8)^{sh}. CD spectrum in H$_2$O [ν_{max}, 10^3 cm^{-1} ($\Delta\varepsilon$)]: 19.57 (−8.63), 26.18 (+7.50), 30.58 (+19.56), 31.6 (+17.4)^{sh}, 33.33 (+16.48), 36.76 (−32.30), 43.67 (−47.54), 46.1 (−41.0)^{sh}, 49.02 (+36.45). Diffuse reflectance spectrum [ν_{max}, 10^3 cm^{-1}]: 19.65, 25.3^{sh}, 28.5^{sh}, 30.1^{sh}, 31.34.

2.3. *Preparation of Λ-[Pd(bpy){Co(aet)$_2$(S-pn)}](NO$_3$)$_3$ (SPd)*

This complex was prepared by a method similar to that used for ***R*Pd**·7H$_2$O using ΛΛ-[Ni{Co(aet)$_2$(*S*-pn)}$_2$]Cl$_4$·6H$_2$O instead of ΔΔ-[Ni{Co(aet)$_2$(*R*-pn)}$_2$]Cl$_4$·6H$_2$O. Yield: 0.33 g (77% based on Co). Anal. Calcd for C$_{17}$H$_{44}$N$_9$O$_{16}$S$_2$CoPd (***S*Pd**·7H$_2$O): C, 23.74; H, 5.16; N, 14.66%. Found: C, 23.73; H, 5.17; N, 14.58%. ^{1}H NMR (300 MHz, D$_2$O), $\delta = 1.40$ (s, 3H, pn), 2.14 (t, 2H, $J = 13.9$ Hz, aet), 2.43 (t, 1H, $J = 13.6$ Hz, pn), 2.63 (d, 2H, $J = 13.9$ Hz, aet), 3.00 (d, 2H, $J = 13.7$ Hz, pn), 3.52 (d, 2H, $J = 13.6$ Hz, aet), 3.66 (t, 2H, $J = 13.2$ Hz, aet), 7.83 (t, 2H, $J = 6.0$ Hz, bpy), 8.33 (t, 2H, $J = 7.9$ Hz, bpy), 8.43 (d, 2H, $J = 7.9$ Hz, bpy), 8.91 (d, 2H, $J = 5.3$ Hz, bpy). UV–Vis spectrum in H$_2$O [ν_{max}, 10^3 cm^{-1} (log ε/M^{-1} dm^3 cm^{-1})]: 20.04 (2.41), 26.1 (3.2)^{sh}, 29.5 (3.9)^{sh}, 31.2 (4.3)^{sh}, 32.47 (4.41), 35.7 (4.3)^{sh}, 43.9 (4.8)^{sh}. CD spectrum in H$_2$O [ν_{max}, 10^3 cm^{-1} ($\Delta\varepsilon$)] 19.57 (+8.50), 26.32 (−8.09), 30.58 (−19.58), 31.6 (−17.2)^{sh}, 33.33 (−16.18), 36.76 (+34.71), 43.86 (+49.84), 46.1 (+43.1)^{sh}, 49.02 (−34.83). Diffuse reflectance spectrum [ν_{max}, 10^3 cm^{-1}]: 19.65, 25.2^{sh}, 28.5^{sh}, 30.1^{sh}, 31.25.

2.4. *Preparation of [Pd(bpy){Co(aet)$_2$(R-pn)}][Pt(bpy){Co(aet)$_2$(S-pn)}](NO$_3$)$_6$ (RPdSPt)*

***S*Pt**·7H$_2$O (0.24 g, 0.25 mM) in 20 cm^3 of H$_2$O was added to a dark red solution containing ***R*Pd**·7H$_2$O (0.22 g, 0.25 mM) in 20 cm^3 of H$_2$O. After the reaction was allowed to stand at 25°C for several days, reddish brown crystals (0.36 g, 88% yield based on Co) were

collected by filtration. Anal. Calcd for $C_{34}H_{68}N_{18}O_{22}S_4Co_2PdPt$ (***R*Pd*S*Pt**·$4H_2O$): C, 25.07; H, 4.21; N, 15.48%. Found: C, 25.08; H, 4.19; N, 15.43%. ^{1}H NMR (300 MHz, D_2O), Δ = 1.41 (s, 6H, pn/***R*Pd** + pn/***S*Pt**), 2.12–2.32 (m, 4H, aet/***R*Pd** + aet/***S*Pt**), 2.40–2.49 (m, 2H, pn/***R*Pd** + pn/***S*Pt**), 2.64 (d, 2H, J = 13.4 Hz, aet/***R*Pd**), 2.76 (d, 2H, J = 12.8 Hz, aet/***S*Pt**), 2.97–3.06 (m, 4H, pn/***R*Pd** + pn/***S*Pt**), 3.38 (d, 2H, J = 13.6 Hz, aet/***S*Pt**), 3.54 (d, 2H, J = 13.6 Hz, aet/***R*Pd**), 3.63–3.77 (m, 4H, aet/***R*Pd** + aet/***S*Pt**), 7.83–7.93 (m, 4H, bpy/***R*Pd** + bpy/***S*Pt**), 8.32–8.49 (m, 8H, bpy/***R*Pd** + bpy/***S*Pt**), 8.92 (d, 2H, J = 5.5 Hz, bpy/***R*Pd**), 9.11 (d, 2H, J = 5.5 Hz, bpy/***S*Pt**). UV–Vis spectrum in H_2O [ν_{max}, 10^3 cm^{-1} (log ε/M^{-1} dm^3 cm^{-1})]: 20.00 (2.71), 26.0 (3.4)^{sh}, 29.0 (4.0)^{sh}, 31.35 (4.60), 32.47 (4.64), 35.7 (4.5)^{sh}, 38.2 (4.6)^{sh}, 41.7 (4.8)^{sh}, 44.0 (4.9)^{sh}. CD spectrum in H_2O [ν_{max}, 10^3 cm^{-1} (Δ ε)]: 25.64 (+13.32), 28.90 (−1.68), 30.49 (+5.63), 31.25 (+4.81), 32.8 (−4.6)^{sh}, 36.36 (−45.34), 40.32 (+8.56), 42.92 (−13.19), 46.0 (+13.8)^{sh}, 48.78 (+64.36). Diffuse reflectance spectrum [ν_{max}, 10^3 cm^{-1}]: 19.76, 27.0^{sh}, 30.58, 31.7^{sh}.

2.5. *Preparation of [Pt(bpy){Co(aet)$_2$(R-pn)}][Pd(bpy){Co(aet)$_2$(S-pn)}](NO$_3$)$_6$ (RPtSPd)*

The same synthetic procedure as for the preparation of ***R*Pd*S*Pt** was employed, except that equimolar amounts of ***R*Pt**·$7H_2O$ and ***S*Pd**·$7H_2O$ were used instead of equimolar amounts of ***R*Pd**·$7H_2O$ and ***S*Pt**·$7H_2O$. Yield = 0.34 g (84% based on Co). Anal. Calcd for $C_{34}H_{68}N_{18}O_{22}S_4Co_2PdPt$ (***R*Pt*S*Pd**·$4H_2O$): C, 25.07; H, 4.21; N, 15.48%. Found: C, 25.10; H, 4.21; N, 15.41%. ^{1}H NMR (300 MHz, D_2O), δ = 1.42 (s, 6H, pn/***R*Pt** + pn/***S*Pd**), 2.13–2.32 (m, 4H, aet/***R*Pt** + aet/***S*Pd**), 2.40–2.49 (m, 2H, pn/***R*Pd** + pn/***S*Pt**), 2.65 (d, 2H, J = 13.4 Hz, aet/***S*Pd**), 2.77 (d, 2H, J = 12.8 Hz, aet/***R*Pt**), 2.97–3.06 (m, 4H, pn/***R*Pd** + pn/***S*Pt**), 3.38 (d, 2H, J = 13.6 Hz, aet/***R*Pt**), 3.54 (d, 2H, J = 13.6 Hz, aet/***S*Pd**), 3.64–3.77 (m, 4H, aet/***R*Pt** + aet/***S*Pd**), 7.83–7.93 (m, 4H, bpy/***R*Pt** + bpy/***S*Pd**), 8.33–8.49 (m, 8H, bpy/***R*Pt** + bpy/***S*Pd**), 8.92 (d, 2H, J = 5.5 Hz, bpy/***S*Pd**), 9.11 (d, 2H, J = 5.5 Hz, bpy/***R*Pt**). UV–Vis spectrum in H_2O [ν_{max}, 10^3 cm^{-1} (log ε/M^{-1} dm^3 cm^{-1})]: 19.96 (2.71), 26.0 (3.4)^{sh}, 29.0 (4.0)^{sh}, 31.35 (4.61), 32.47 (4.64), 35.7 (4.5)^{sh}, 38.2 (4.6)^{sh}, 41.7 (4.8)^{sh}, 44.0 (4.9)^{sh}. CD spectrum in H_2O [ν_{max}, 10^3 cm^{-1} (Δ ε)]: 25.64 (−13.31), 28.99 (+1.53), 30.58 (−5.57), 31.2 (−4.3)^{sh}, 32.8 (+6.0)^{sh}, 36.50 (+46.79), 40.16 (−8.10), 43.10 (+13.57), 46.0 (−12.2)^{sh}, 48.78 (−59.85). Diffuse reflectance spectrum [ν_{max}, 10^3 cm^{-1}]: 19.76, 27.0^{sh}, 30.58, 31.7^{sh}.

2.6. *Measurements*

Electronic absorption spectra were recorded on a Perkin-Elmer Lambda 19 spectrophotometer and the CD spectra were recorded on a JASCO J-720 spectropolarimeter. These measurements were carried out in aqueous solutions at room temperature. Solid-state CD spectra were measured as KBr disks on a JASCO J-800 spectropolarimeter. Diffuse reflectance spectra were measured with a Perkin-Elmer Lambda 900 spectrophotometer equipped with an integrating sphere apparatus. ^{1}H NMR spectra were recorded on a JEOL JNM-AL300 NMR spectrometer in D_2O using sodium 4,4-dimethyl-4-silapentane-1-sulfonate (DSS) as an internal reference. C, H and N elemental analyses were performed with a Perkin-Elmer 2400 CHN Elemental Analyzer.

2.7. *X-ray structure determination*

Single crystals of ***R*Pd*S*Pt**·$4H_2O$ and ***R*Pt*S*Pd**·$4H_2O$ were used for data collection on a Rigaku AFC5S automated four-circle diffractometer with graphite-monochromated Mo *Kα*

(λ = 0.71069 Å) radiation. Cell constants and an orientation matrix for data collection were obtained from a least-squares refinement using the setting angles of 25 carefully centered reflections in the range $14° < \theta < 15°$. The data were collected at 296 ± 1 K using the ω-2θ scan technique to a maximum 2θ value of 55°. The weak reflections ($I < 10.0\sigma(I)$) were rescanned (maximum of three scans) and the counts were accumulated to ensure good counting statistics. Stationary background counts were recorded on each side of a reflection. The ratio of peak counting time to background counting time was 2 : 1. The intensities of three representative reflections were measured after every 150 reflections. Over the course of data collection, the standards decreased by <0.4%. Polynomial correction factors were applied to the data to account for this phenomenon. Empirical absorption corrections based on azimuthal scans of several reflections were applied. The data were corrected for Lorentz and polarization effects. The crystal data and structural refinement parameters are summarized in table 1. The structures were solved by direct methods and expanded using Fourier techniques [12, 13]. Non-hydrogen atoms were refined anisotropically. All hydrogens, except those of waters which were not included in any of the structural models because their positions could not be determined precisely, were placed in calculated positions and were refined with a riding model. The final cycle of full-matrix least-squares refinement on F^2 was based on observed reflections and variable parameters, and converged with the unweighted and weighted agreement factors R and Rw. The absolute structure was deduced based on the Flack parameter, refined using Friedelspairs [14]. Neutral atom scattering factors were taken from Cromer and Waber [15]. Anomalous dispersion effects were included in Fc; the values for $\Delta f'$ and $\Delta f''$ were those of Creagh and McAuley [16–18]. All calculations were performed using the CrystalStructure crystallographic software package of Molecular Structure Corporation [19, 20]. Relevant bond distances and angles are listed in table 2.

Table 1. Crystallographic data for ***R*PdS*P*t**·4H_2O and ***R*PtS*P*d**·4H_2O.

	***R*PdS*P*t**·4H_2O	***R*PtS*P*d**·4H_2O
Formula	$C_{34}H_{68}Co_2N_{18}O_{22}PdPtS_4$	$C_{34}H_{68}Co_2N_{18}O_{22}PdPtS_4$
Formula weight	1628.62	1628.62
Space group	P_1	P_1
a (Å)	7.948(2)	7.946(2)
b (Å)	12.046(2)	12.047(2)
c (Å)	15.739(3)	15.734(3)
α (°)	104.03(2)	104.01(2)
β (°)	91.54(2)	91.56(2)
γ (°)	98.30(2)	98.29(2)
V (Å^3)	1443.7(6)	1443.1(5)
Z	1	1
Dc (g cm^{-3})	1.873	1.874
μ (cm^{-1})	35.101	35.116
Tot. reflections	13288	13288
No. of variables	800	800
R_1 [$I > 2\sigma(I)$]	0.0303	0.0276
R (all data)	0.0323	0.0290
wR_2 (all data)	0.0749	0.0699
Goodness-of fit on F^2	1.018	1.030
Flack parameter	−0.002(2)	−0.003(2)

Table 2. Selected bond distances (Å) and angles (°) for ***R*Pd*S*Pt**·4H_2O and ***R*Pt*S*Pd**·4H_2O.

	***R*Pd*S*Pt**·4H_2O	***R*Pt*S*Pd**·4H_2O
Co(1)–S(1)	2.233(2)	2.2311(18)
Co(1)–S(2)	2.251(2)	2.2531(19)
Co(1)–N(1)	1.972(5)	1.977(5)
Co(1)–N(2)	1.988(5)	1.982(5)
Co(1)–N(3)	1.997(5)	1.983(5)
Co(1)–N(4)	1.990(5)	1.984(5)
Co(2)–S(3)	2.233(3)	2.237(3)
Co(2)–S(4)	2.258(3)	2.255(3)
Co(2)–N(7)	1.980(5)	1.981(5)
Co(2)–N(8)	1.988(5)	1.990(5)
Co(2)–N(9)	1.988(5)	1.992(5)
Co(2)–N(10)	1.992(5)	2.002(5)
Pd(1)–S(1)	2.275(2)	2.2746(18)
Pd(1)–S(2)	2.3012(19)	2.3022(17)
Pd(1)–N(5)	2.069(6)	2.070(5)
Pd(1)–N(6)	2.068(6)	2.065(5)
Pt(1)–S(3)	2.281(3)	2.278(3)
Pt(1)–S(4)	2.298(3)	2.296(2)
Pt(1)–N(11)	2.030(8)	2.035(7)
Pt(1)–N(12)	2.054(8)	2.054(8)
S(1)–Co(1)–S(2)	85.41(8)	85.42(7)
S(1)–Co(1)–N(1)	87.85(14)	87.92(12)
S(1)–Co(1)–N(2)	89.52(14)	89.54(13)
S(1)–Co(1)–N(3)	93.56(15)	93.73(13)
S(1)–Co(1)–N(4)	178.81(17)	179.00(15)
S(2)–Co(1)–N(1)	89.32(14)	89.32(13)
S(2)–Co(1)–N(2)	88.20(15)	88.00(14)
S(2)–Co(1)–N(3)	178.64(16)	178.59(15)
S(2)–Co(1)–N(4)	95.70(16)	95.50(15)
N(1)–Co(1)–N(2)	176.5(2)	176.45(19)
N(1)–Co(1)–N(3)	91.5(2)	91.77(19)
N(1)–Co(1)–N(4)	91.7(2)	91.70(19)
N(2)–Co(1)–N(3)	90.9(2)	90.9(2)
N(2)–Co(1)–N(4)	90.9(2)	90.88(19)
N(3)–Co(1)–N(4)	85.3(2)	85.36(19)
S(3)–Co(2)–S(4)	85.31(9)	85.26(8)
S(3)–Co(2)–N(7)	88.32(14)	88.24(13)
S(3)–Co(2)–N(8)	89.51(15)	89.47(13)
S(3)–Co(2)–N(9)	94.14(15)	94.08(14)
S(3)–Co(2)–N(10)	178.43(17)	178.20(15)
S(4)–Co(2)–N(7)	89.63(15)	89.51(14)
S(4)–Co(2)–N(8)	88.18(16)	88.32(14)
S(4)–Co(2)–N(9)	178.49(17)	178.76(15)
S(4)–Co(2)–N(10)	96.19(16)	96.43(15)
N(7)–Co(2)–N(8)	177.0(2)	176.97(18)
N(7)–Co(2)–N(9)	91.8(2)	91.52(19)
N(7)–Co(2)–N(10)	91.2(2)	91.16(18)
N(8)–Co(2)–N(9)	90.4(2)	90.6(2)
N(8)–Co(2)–N(10)	91.0(2)	91.19(19)
N(9)–Co(2)–N(10)	84.4(2)	84.24(19)
S(1)–Pd(1)–S(2)	83.32(7)	83.30(6)
S(1)–Pd(1)–N(5)	96.51(17)	96.86(16)
S(1)–Pd(1)–N(6)	176.07(16)	176.26(15)
S(2)–Pd(1)–N(5)	179.54(19)	179.47(16)
S(2)–Pd(1)–N(6)	100.11(15)	99.98(14)

(*Continued*)

Table 2. (*Continued*).

	***R*PdS*S*Pt·4H$_2$O**	***R*PtS*S*Pd·4H$_2$O**
N(5)–Pd(1)–N(6)	80.1(3)	79.9(2)
S(3)–Pt(1)–S(4)	83.29(9)	83.40(8)
S(3)–Pt(1)–N(11)	97.0(3)	96.7(3)
S(3)–Pt(1)–N(12)	176.5(3)	176.2(2)
S(4)–Pt(1)–N(11)	178.6(3)	178.8(3)
S(4)–Pt(1)–N(12)	100.0(3)	100.05(19)
N(11)–Pt(1)–N(12)	79.7(4)	79.9(3)
Pd(1)–S(1)–Co(1)	96.24(7)	96.32(6)
Pd(1)–S(2)–Co(1)	95.01(7)	94.94(6)
Pt(1)–S(3)–Co(2)	96.27(9)	96.16(8)
Pt(1)–S(4)–Co(2)	95.10(8)	95.15(8)

3. Results and discussion

3.1. *Crystal structures*

A mixture of equimolar amounts of ***R*Pd**·7H$_2$O and ***S*Pt**·7H$_2$O in H$_2$O crystallized as ***R*Pd*S*Pt**·4H$_2$O in the acentric space group of triclinic *P*1, in contrast to the centric space group of monoclinic $P2_1/c$ or triclinic $P\bar{1}$ for crystals of racemic [Pt(bpy){Co(aet)$_2$(*R*-pn)}]$_{0.5}$[Pt(bpy){Co(aet)$_2$(*S*-pn)}]$_{0.5}$X$_3$·2H$_2$O (X = ClO_4^-, NO_3^-) [5]. An X-ray structural analysis of ***R*Pd*S*Pt**·4H$_2$O revealed the presence of two kinds of discrete trivalent complex cations, six nitrates, and four crystallization waters. As shown in figure 1(a), one of these trivalent complex cations is [Pd(bpy){Co(aet)$_2$(*R*-pn)}]$^{3+}$ and the other is [Pt(bpy){Co(aet)$_2$(*S*-pn)}]$^{3+}$. The absolute configuration of the Co(III) unit in [Pd(bpy){Co(aet)$_2$(*R*-pn)}]$^{3+}$ is Δ, while that in [Pt(bpy){Co(aet)$_2$(*S*-pn)}]$^{3+}$ is Λ. This indicates no rearrangement in dinuclear structures during the crystallization of ***R*Pd*S*Pt**·4H$_2$O. In Δ-[Pd(bpy){Co(aet)$_2$(*R*-pn)}]$^{3+}$, the dihedral angle between the PdS_2 and PdN_2 planes is 2.058°, indicating an approximately square-planar Pd(II). Additionally, the dihedral angle between the PdS_2N_2 square-plane and the CoS_2N_2 equatorial plane is 0.9°. This implies that these two planes are almost coplanar. In Λ-[Pt(bpy){Co(aet)$_2$(*S*-pn)}]$^{3+}$, analogously, the PtN_2S_2 chromophore forms nearly a square-plane (dihedral angle between PtS_2 and PtN_2 planes, 2.041°), and the PtS_2N_2 square-plane and CoS_2N_2 equatorial plane retain coplanarity (dihedral angle, 2.1°). These structural characteristics are essentially identical to those for other doubly sulfur-bridged dinuclear Co(III)–M(II) complexes [1–7]. The bpy framework of Δ-[Pd(bpy){Co(aet)$_2$(*R*-pn)}]$^{3+}$ is placed in a face-to-face arrangement with that of Λ-[Pt(bpy){Co(aet)$_2$(*S*-pn)}]$^{3+}$. As a result, these two complex cations with imperfect enantiomorphisms form a 1 : 1 π–π stacked unit, in which the interplanar distance and angle between two bpy frameworks are 3.52 Å and 2.1°, respectively. The interplanar distance between the two bpy frameworks in ***R*Pd*S*Pt**·4H$_2$O is somewhat elongated as compared with that in racemic [Pt(bpy){Co(aet)$_2$(*R*-pn)}]$_{0.5}$[Pt(bpy){Co(aet)$_2$(*S*-pn)}]$_{0.5}$(NO$_3$)$_3$·2H$_2$O (3.47 Å) [5]. This may suggest that the stereospecific π–π stacking interactions in pseudo-enantiomers with different d^8 metal centers are slightly weaker compared with those in the genuine enantiomers. On the other hand, the 1 : 1 π–π stacked unit between pseudo-enantiomeric complex cations, Δ-[Pd(bpy){Co(aet)$_2$(*R*-pn)}]$^{3+}$ and Λ-[Pt(bpy){Co(aet)$_2$(*S*-pn)}]$^{3+}$, does not develop into a linear chain with further π–π stacking contacts like that in racemic [Pt(bpy){Co(aet)$_2$(*R*-pn)}]$_{0.5}$[Pt(bpy){Co(aet)$_2$(*S*-pn)}]$_{0.5}$X$_3$·2H$_2$O [5]. A similar trend in structural

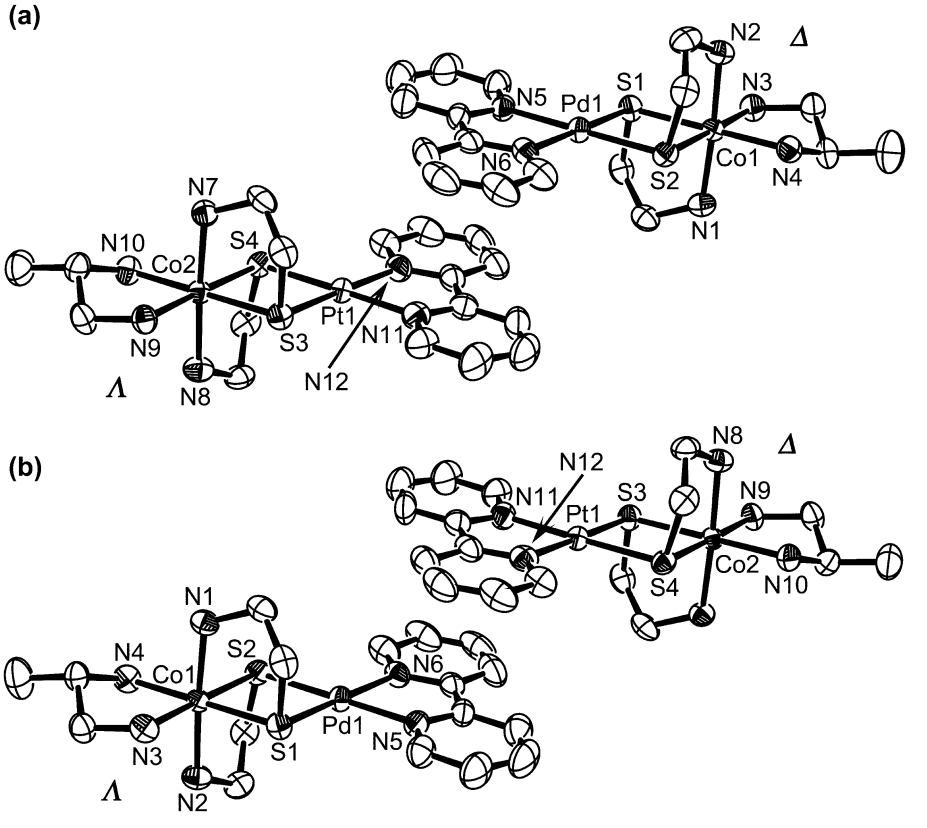

Figure 1. Perspective views of the 1 : 1 π–π stacked units between the pseudo-enantiomeric complex cations in (a) ***R*Pd*S*Pt**·$4H_2O$ and (b) ***R*Pt*S*Pd**·$4H_2O$. Thermal ellipsoids are shown at 50% probability.

characteristics is also observed for ***R*Pt*S*Pd**·$4H_2O$ with an interplanar distance of 3.52 Å between the two bpy frameworks [figure 1(b)]. It can be concluded, therefore, that stereospecific π–π stacking interactions, which have been demonstrated for enantiomeric complex cations with perfect mirror images, are applicable to assemblies between pseudo-enantiomers with different d^8 metal centers, Δ-[M(bpy){Co(aet)$_2$(*R*-pn)}]$^{3+}$ (M = Pd or Pt) and Λ-[M′(bpy){Co(aet)$_2$(*S*-pn)}]$^{3+}$ (M′ ≠ M, M′ = Pd or Pt).

3.2. *Characterization*

In D_2O, ***R*Pd*S*Pt** exhibited ^{1}H NMR signals in the region of 1.3–9.2 ppm. Over the whole region, the signals of ***R*Pd** considerably overlap with those of ***S*Pt**, and hence most signals of ***R*Pd*S*Pt** were observed as multiplets or were unresolved. However, the signals due to 6- and 6′-protons of the bpy frameworks in ***R*Pd** and ***S*Pt** were well-resolved and appear as doublets at $\delta = 8.92$ and 9.11. The former signal at $\delta = 8.92$ is assigned to the bpy ligand coordinated to Pd(II) in ***R*Pd** and the latter signal is ascribed to the one coordinated to Pt(II) in ***S*Pt** [1, 5]. Integrated intensities for these two signals coincide well with each other and bear out the 1 : 1 pseudo-racemic crystal formula for

R*Pd*S*Pt**. Additionally, the spectral profile of ***R*Pd*S*Pt** is closely related to that of both ***R*Pd** and ***S*Pt**. There are no significant shifts and broadenings in any of the remaining bpy proton signals. A similar trend is also observed for the ^{1}H NMR spectrum of ***R*Pt*S*Pd**. It seems, therefore, that each of the complex cations in ***R*Pd*S*Pt** or ***R*Pt*S*Pd** is free from π–π stacking interactions in solutions with a concentration of 10^{-2} M dm^{-3}. As the measurements for the electronic absorption and CD spectra were collected on further diluted concentrations of 10^{-2}–10^{-5} M dm^{-3}, it is predictable that each of the complex cations in ***R*Pd*S*Pt** or ***R*Pt*S*Pd** exists independently with respect to such intermolecular interactions. It can be rationally considered therefore that the observed electronic absorption and CD spectra of ***R*Pd*S*Pt** (R*Pt*S*Pd**) are reproducible by the arithmetic

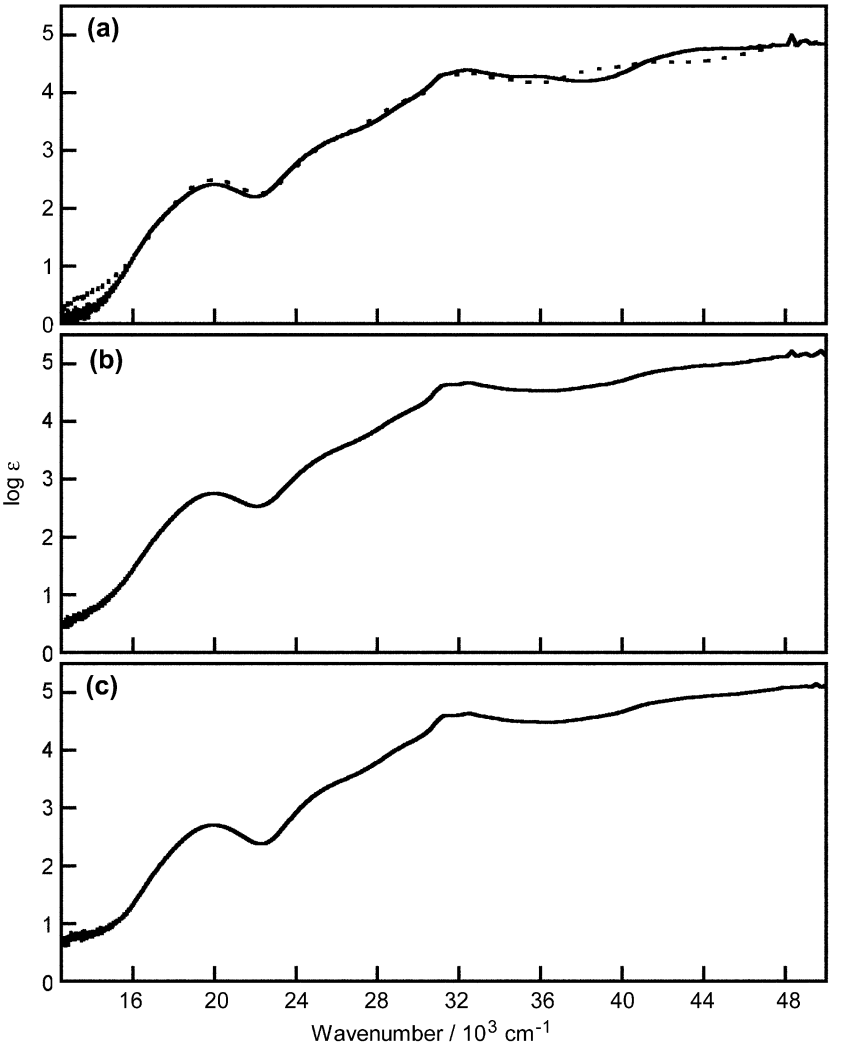

Figure 2. Electronic absorption spectra of (a) ***R*Pd**·7H$_2$O (solid line) and ***S*Pt**·7H$_2$O (broken line), and (c) ***R*Pd*S*Pt**·4H$_2$O, together with (b) estimated electronic absorption spectrum by superimposition of the observed ones for ***R*Pd**·7H$_2$O and ***S*Pt**·7H$_2$O. The path length was 1.0 cm and the concentrations were 10^{-2}–10^{-5} M dm^{-3}.

superimposition of corresponding spectra from the two constituent complex cations, ***R*Pd** and ***S*Pt** (***R*Pt** and ***S*Pd**). As shown in figures 2 and 3, in fact, the electronic absorption and CD spectra of ***R*Pd*S*Pt** (***R*Pt*S*Pd**) are almost identical with the calculated ones. In addition, the CD spectral profiles of ***R*Pd*S*Pt** (***R*Pt*S*Pd**) in solution are essentially consistent with those in the solid state (see figure S1, see online supplemental material at http://dx.doi.org/10.1080/00958972.2014.919387). This result supports the stereoselectivities of ***R*Pd*S*Pt** (***R*Pt*S*Pd**) in solution as well as in the solid state. In particular, the CD signals of these pseudo-racemic crystals sharply contrast with the corresponding spectra of the racemic crystals such as $[Pt(bpy)\{Co(aet)_2(R\text{-pn})\}]_{0.5}[Pt(bpy)\{Co(aet)_2(S\text{-pn})\}]_{0.5}X_3\cdot 2H_2O$, in which the two enantiomeric complex cations negate the CD signals of the other [5].

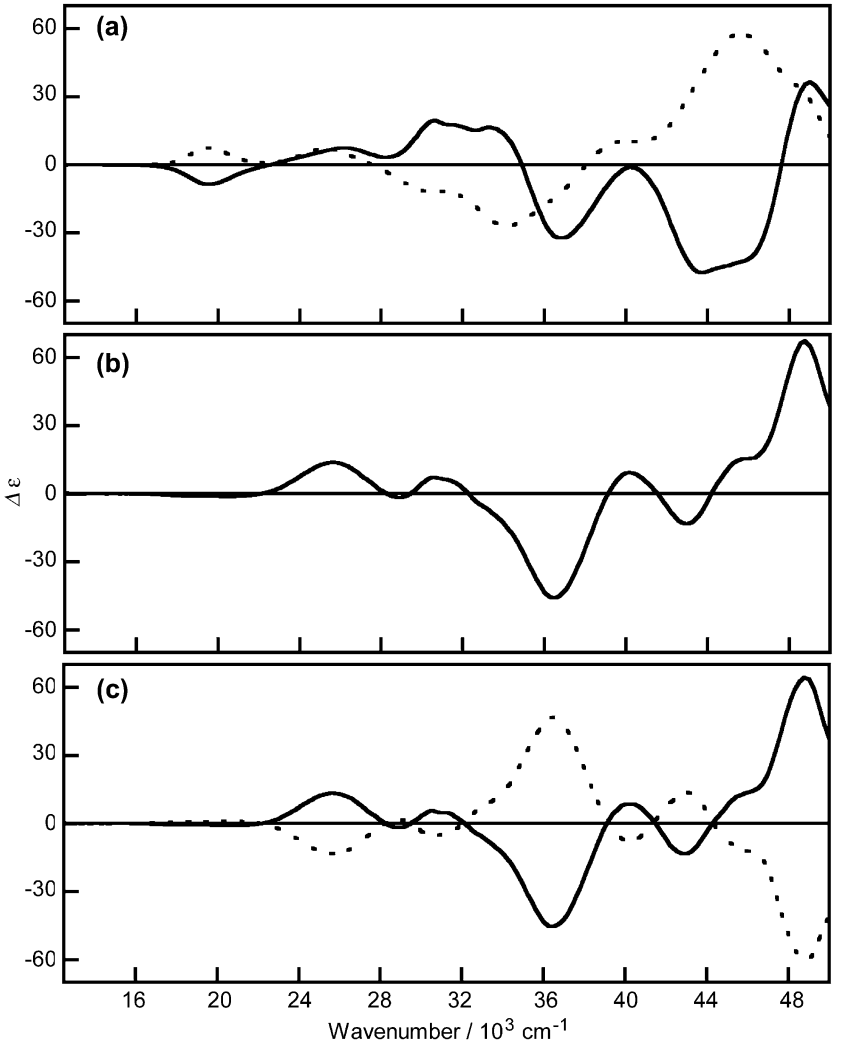

Figure 3. CD spectra of (a) ***R*Pd**·$7H_2O$ (full line) and ***S*Pt**·$7H_2O$ (broken line), and (c) ***R*Pd*S*Pt**·$4H_2O$ (full line) and ***R*Pt*S*Pd**·$4H_2O$ (broken line), together with (b) estimated CD spectrum by superimposition of the observed ones for ***R*Pd**·$7H_2O$ and ***S*Pt**·$7H_2O$. The path length was 1.0 cm and the concentrations were 10^{-2}–10^{-5} M dm^{-3}.

The diffuse reflectance spectrum of ***R*Pd*S*Pt**·$4H_2O$ (***R*Pt*S*Pd**·$4H_2O$) roughly corresponds to its absorption spectrum in H_2O, but some essential differences can be seen between the two spectra (figure 4). In the reflectance spectrum of ***R*Pd*S*Pt**·$4H_2O$ (***R*Pt*S*Pd**·$4H_2O$), for instance, the π–π^* bands due to the localized electronic transitions from bpy are considerably shifted toward lower energy in spite of the slightly lower-energy shift of the d–d band. In the 25–29 × 10^3 cm^{-1} region, furthermore, the absorption spectrum of ***R*Pd*S*Pt**·$4H_2O$ (***R*Pt*S*Pd**·$4H_2O$) showed two well-resolved shoulders at 26.0 and 29.0 × 10^3 cm^{-1}, while the reflectance spectrum had one broad shoulder at 27.0 × 10^3 cm^{-1}. A similar trend was observed for racemic crystals of $[Pt(bpy)\{Co(aet)_2(R\text{-pn})\}]_{0.5}[Pt(bpy)\{Co(aet)_2(S\text{-pn})\}]_{0.5}X_3\cdot 2H_2O$ (X = NO_3, ClO_4) and $[Pt(bpy)\{Co(\text{D-pen})_2\}]_{0.5}[Pt(bpy)\{Co(\text{L-pen})_2\}]_{0.5}X\cdot nH_2O$ (X = I, NO_3, ClO_4, BF_4) with dimeric π–π stacking arrangements [5, 6, 21]. In addition, analogous bands were also observed for doubly sulfur-bridged d^8 metal aromatic diimine complexes with intra- and/or intermolecular π–π stacking arrangements

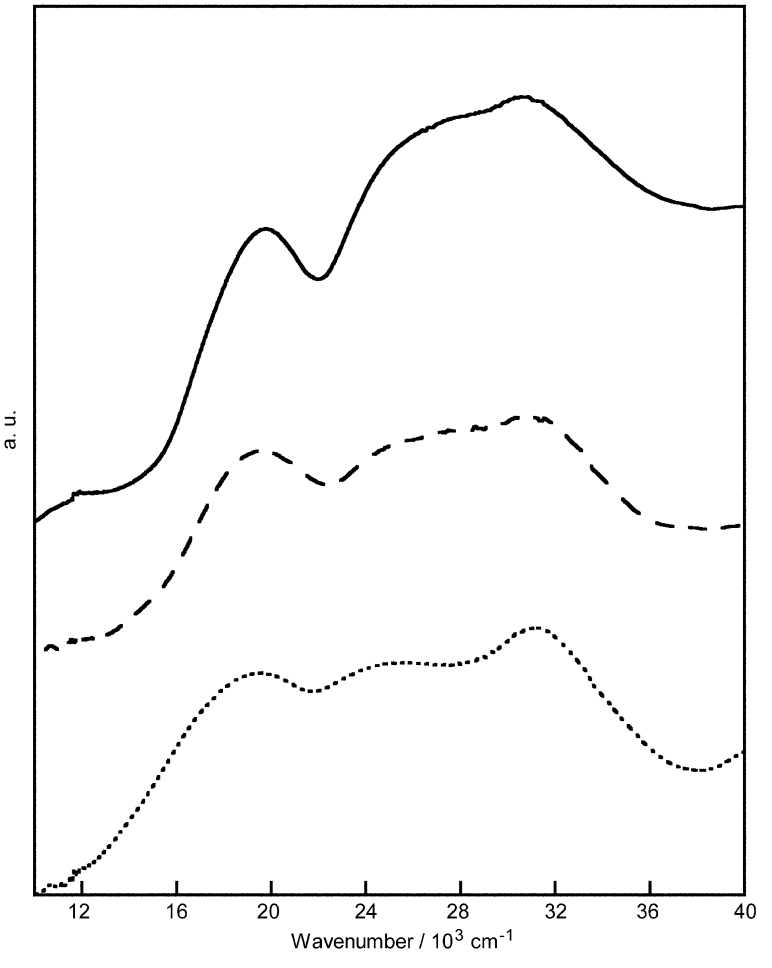

Figure 4. Diffuse reflectance spectra of ***R*Pd**·$7H_2O$ (dotted line), ***S*Pt**·$7H_2O$ (broken line), and ***R*Pd*S*Pt**·$4H_2O$ (full line).

[22–24]. It seems, therefore, that the broad band around 27×10^3 cm^{-1} originates from the formation of a 1 : 1 π–π stacked unit between the pseudo-enantiomeric complex cations, Δ-[Pd(bpy){Co(aet)$_2$(*R*-pn)}]$^{3+}$ and Λ-[Pt(bpy){Co(aet)$_2$(*S*-pn)}]$^{3+}$, in ***R*Pd*S*Pt**·4H$_2$O (Δ-[Pt(bpy){Co(aet)$_2$(*R*-pn)}]$^{3+}$ and Λ-[Pd(bpy){Co(aet)$_2$(*S*-pn)}]$^{3+}$, in ***R*Pt*S*Pd**·4H$_2$O).

4. Conclusion

The reaction of [Ni{Co(aet)$_2$(*R*-pn)}$_2$]$^{4+}$ ([Ni{Co(aet)$_2$(*S*-pn)}$_2$]$^{4+}$), in which Δ-*cis(S)*-[Co(aet)$_2$(*R*-pn)]$^+$ (Λ-*cis(S)*-[Co(aet)$_2$(*S*-pn)]$^+$) units are bidentate metalloligands with [PdCl$_2$(bpy)] in the presence of nitrate anions, gave an optically active S-bridged dinuclear complex, Δ-[Pd(bpy){Co(aet)$_2$(*R*-pn)}](NO$_3$)$_3$ (Λ-[Pd(bpy){Co(aet)$_2$(*S*-pn)}](NO$_3$)$_3$), whose structure is similar to the previously reported complex, Δ-[Pt(bpy){Co(aet)$_2$(*R*-pn)}](NO$_3$)$_3$ (Λ-[Pt(bpy){Co(aet)$_2$(*S*-pn)}](NO$_3$)$_3$). Mixing these pseudo-enantiomers with different d^8 metal centers, Δ-[M(bpy){Co(aet)$_2$(*R*-pn)}]$^{3+}$ (M = Pd or Pt) and Λ-[M′(bpy){Co(aet)$_2$(*S*-pn)}]$^{3+}$ (M′ ≠ M, M′ = Pd or Pt) in molar ratio 1 : 1 in H$_2$O led to the formation of pseudo-racemic crystals, [M(bpy){Co(aet)$_2$(*R*-pn)}][M′(bpy){Co(aet)$_2$(*S*-pn)}](NO$_3$)$_6$·4H$_2$O. In these pseudo-racemic crystals, Δ-[M(bpy){Co(aet)$_2$(*R*-pn)}]$^{3+}$ and Λ-[M′(bpy){Co(aet)$_2$(*S*-pn)}]$^{3+}$ interact stereospecifically with each other through π-conjugated systems to form pseudo-dimeric structures. These structural characteristics are reflected in their spectral behaviors.

Supplementary material

CCDC-960228 for ***R*Pd*S*Pt**·4H$_2$O and 960229 for ***R*Pt*S*Pd**·4H$_2$O contain the supplementary crystallographic data for this paper. These data can be obtained free of charge at www.ccdc.cam.ac.uk/conts/retrieving.html [or from the Cambridge Crystallographic Data Center, 12 Union Road, Cambridge CB2 1EZ, UK; Fax: +44 1223 336 033; E-mail: deposit@ccdc.cam.ac.jk].

References

[1] Y. Yamada, M. Uchida, Y. Miyashita, K. Fujisawa, T. Konno, K. Okamoto. *Bull. Chem. Soc. Jpn.*, **73**, 913 (2000).
[2] Y. Yamada, Y. Maeda, T. Konno, K. Fujisawa, K. Okamoto. *Bull. Chem. Soc. Jpn.*, **73**, 1831 (2000).
[3] Y. Yamada, M. Uchida, M. Fujita, Y. Miyashita, K. Okamoto. *Polyhedron*, **22**, 1507 (2003).
[4] Y. Yamada, K. Okamoto. *Inorg. Chim. Acta*, **359**, 3963 (2006).
[5] Y. Yamada, M. Noda, M. Inoue, Y. Miyashita, K. Okamoto, M. Koikawa, T. Tokii. *J. Coord. Chem.*, **60**, 607 (2007).
[6] Y. Yamada, M. Inoue, Y. Miyashita, K. Okamoto, M. Koikawa, T. Tokii. *Polyhedron*, **26**, 2749 (2007).
[7] Y. Yamada, M. Inoue, K. Okamoto. *J. Coord. Chem.*, **61**, 1385 (2008).
[8] Y. Yamada, Y. Maeda, Y. Miyashita, K. Fujisawa, T. Konno, K. Okamoto. *Bull. Chem. Soc. Jpn.*, **73**, 1219 (2000).
[9] N. Baidya, D. Ndreu, M. Olmstead, K. Mascharak. *Inorg. Chem.*, **30**, 2448 (1991).
[10] R.H. Herber, M. Croft, M.J. Coyer, B. Bilash, A. Sahiner. *Inorg. Chem.*, **33**, 2422 (1994).
[11] K. Okamoto, Y. Yoshinari, Y. Yamada, N. Sakagami, T. Konno. *Bull. Chem. Soc. Jpn.*, **71**, 1363 (1998).
[12] SIR92: A. Altomare, G. Cascarano, C. Giacovazzo, A. Guagliardi, M. Burla, G. Polidori, M. Camalli. *J. Appl. Cryst.*, **27**, 435 (1994).

[13] P.T. Beurskens, G. Admiraal, G. Beurskens, W.P. Bosman, R. de Gelder, R. Israel, J.M.M. Smits. *DIRDIF99. The DIRDIF 99 Program System*, Technical Report of the Crystallography Laboratory, University of Nijmegen, Nijmegen (1999).
[14] H.D. Flack. *Acta Cryst.*, **A39**, 876 (1983).
[15] D.T. Cromer, J.T. Waber (Eds.). *International Tables for X-ray Crystallography*, Vol. IV, The Kynoch Press, Birmingham, Table 2.2 A (1974).
[16] J.A. Ibers, W.C. Hamilton. *Acta Cryst.*, **17**, 781 (1964).
[17] D.C. Creagh, W.J. McAuley. In *International Tables for Crystallography*, A.J.C. Wilson (Ed.), Vol. C, pp. 219–222, Kluwer Academic Publishers, Boston, MA (1992).
[18] D.C. Creagh, J.H. Hubbell. In *International Tables for Crystallography*, A.J.C. Wilson (Ed.), Vol. C, pp. 200–206, Kluwer Academic Publishers, Boston, MA (1992).
[19] *CrystalStructure 4.0: Crystal Structure Analysis Package*, Rigaku Corporation, Tokyo 196-8666, Japan (2000–2010).
[20] J.R. Carruthers, J.S. Rollett, P.W. Betteridge, D. Kinna, L. Pearce, A. Larsen, E. Gabe. *CRYSTALS Issue 11*, Chemical Crystallography Laboratory, Oxford (1999).
[21] Y. Yamada, M. Kono, Y. Miyoshi, T. Nagasaki, M. Koikawa, T. Tokii. *J. Coord. Chem.*, **63**, 742 (2010).
[22] Y. Yamada, K. Okamoto. *Chem. Lett.*, **28**, 315 (1999).
[23] Y. Yamada, K. Fujisawa, K. Okamoto. *Bull. Chem. Soc. Jpn.*, **73**, 2067 (2000).
[24] Y. Yamada, K. Fujisawa, K. Okamoto. *Bull. Chem. Soc. Jpn.*, **73**, 2297 (2000).